Metastable discrete time-crystal resonances in a dissipative central spin system

Albert Cabot [1,*] Federico Carollo [1] and Igor Lesanovsky [1,2]

[1]*Institut für Theoretische Physik, Eberhard Karls Universität Tübingen, Auf der Morgenstelle 14, 72076 Tübingen, Germany*
[2]*School of Physics and Astronomy and Centre for the Mathematics and Theoretical Physics of Quantum Non-Equilibrium Systems, The University of Nottingham, Nottingham, NG7 2RD, United Kingdom*

We consider the nonequilibrium behavior of a central spin system where the central spin is periodically reset to its ground state. The quantum-mechanical evolution under this effectively dissipative dynamics is described by a discrete-time quantum map. Despite its simplicity this problem shows surprisingly complex dynamical features. In particular, we identify several metastable time-crystal resonances. Here the system does not relax rapidly to a stationary state but undergoes long-lived oscillations with a period that is an integer multiple of the reset period. At these resonances the evolution becomes restricted to a low-dimensional state space within which the system undergoes a periodic motion. Generalizing the theory of metastability in open quantum systems, we develop an effective description for the evolution within this long-lived metastable subspace and show that in the long-time limit a nonequilibrium stationary state is approached. Our study links to timely questions concerning emergent collective behavior in the "prethermal" stage of a dissipative quantum many-body evolution and may establish an intriguing link to the phenomenon of quantum synchronization.

I. INTRODUCTION

The interplay of coherent and incoherent processes in interacting driven-dissipative quantum systems can lead to nonequilibrium phases and symmetry breaking [1–7], the emergence of long relaxation timescales [8–10], or dynamical hysteresis [11]. Time crystals are an example of a genuine nonequilibrium phase [12–14], in which discrete or continuous time-translation symmetry is spontaneously broken. Such phases were initially reported for Hamiltonian systems subject to periodic driving [15–17], and later also found in driven-dissipative scenarios [18–24]. They have also been reported in a prethermal [25–28] or in a prestationary [29–33] regime, manifesting in long-lived subharmonic collective oscillations. Emergent long timescales are also common in the dynamics of open quantum systems [9,34–39]. They occur typically in the vicinity of dissipative phase transitions (DPTs), as a finite-size manifestation of the closure of the Liouvillian spectral gap [40–42]. Similarly, the emergence of multistability and symmetry broken phases can be accompanied by such long-lived dynamical response [42]. Metastable dynamics, i.e., prestationary regimes characterized by relaxation into long-lived states [9], may also emerge independently of any stationary phase transition, as a purely dynamical phenomenon. This is, e.g., the case in constrained spin models [43,44]. Such long-lived excitations can impose their frequency to the system, leading to quantum synchronization phenomena [37,45–47].

In this paper, we consider an open quantum dynamics realized by interrupting the coherent evolution of a system with the periodic resetting of some of its degrees of freedom [see Fig. 1(a)]. By focusing on a central spin system, we show that this dissipative discrete dynamics can give rise to novel nonequilibrium phenomena. In particular, we observe the emergence of metastable resonances, in which the system displays long-lived oscillations, with a period that is locked to a multiple of the reset period [see Figs. 1(b) and 2], and in which "heating" towards an infinite-temperature state is avoided. To describe the dynamics at these resonances, we develop an effective theory in which the time-translation symmetry breaking is decoupled from an emergent classical nonequilibrium dynamics accounting for the (slow) eventual decay towards the stationary state. Our results demonstrate the emergence of nonequilibrium behavior that is substantially different from conventional phase transitions and "prethermal" or metastable time-crystalline phases. The observed behavior is metastable in the sense that its manifestation requires large system sizes, and is seemingly not related to a (standard) nonequilibrium phase transition. Upon varying the system size, the metastable resonances can become weaker or stronger, and do not smoothly approach a well-determined thermodynamic limit.

II. DISSIPATIVE CENTRAL SPIN MODEL

We consider a central spin model in which N system spins interact with a central one. Such models are relevant in the description of hyperfine interactions between quantum dots [48] or nitrogen-vacancy centers in diamond [49] and their environment. Moreover, they are known to display interesting dynamical phenomena both in closed and driven-dissipative scenarios [8,50–53]. Our starting point is an XX Hamiltonian ($\hbar = 1$) where all system spins are resonantly driven with a Rabi frequency ω and coupled with the same strength g to the central spin [see Fig. 1(a)]:

$$\hat{H} = \omega \hat{J}_x + g(\hat{J}_+ \hat{\sigma}_- + \hat{J}_- \hat{\sigma}_+). \tag{1}$$
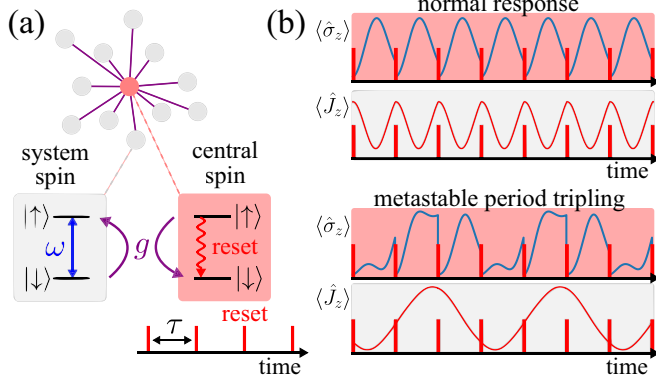
*Corresponding author: albert.cabot@itp.uni-tuebingen.de

FIG. 1. Dissipative central spin model. (a) N system spins interact with a central spin for a time period τ after which the latter is reset to the ground state. (b) Long-time dynamics of the magnetization of the central spin, $\langle \hat{\sigma}_z \rangle$, and of the system spins, $\langle \hat{J}_z \rangle$. In the normal response, both the system spins and the central spin approach a steady state that oscillates with the reset period τ (upper panels). In the metastable time-crystal regime, the spins display long-lived oscillations whose period is a multiple of τ; in the present case 3τ (lower panels). Parameters: $N = 30$, $g\tau = 0.2$, and $\omega\tau = 1.5$ (upper panels) or $\omega\tau = 2\pi/3$ (lower panels).

Here $\hat{J}_\alpha = \frac{1}{2}\sum_{j=1}^{N}\hat{\sigma}_\alpha^{(j)}$ and $\hat{J}_\pm = \hat{J}_x \pm i\hat{J}_y$ are collective spin operators and raising/lowering operators, respectively, representing the ensemble of system spins. They are constructed from the Pauli matrices $\hat{\sigma}_\alpha$ ($\alpha = x, y, z$). The central spin is represented through the raising/lowering operators $\hat{\sigma}_\pm = (\hat{\sigma}_x \pm i\hat{\sigma}_y)/2$. The dissipative dynamics emerges from periodically (period τ) resetting to the ground state ($|\downarrow\rangle \langle\downarrow|_c$) the central spin, as illustrated in Fig. 1(a). The reduced density matrix $\hat{\rho}$ for the collective spin at multiples of τ is then given by [54]

$$\hat{\rho}_{n+1} = \mathcal{E}\hat{\rho}_n = \text{Tr}_c[\hat{U}\hat{\rho}_n \otimes |\downarrow\rangle\langle\downarrow|_c \,\hat{U}^\dagger]. \tag{2}$$

Here $\hat{U} = e^{-i\hat{H}\tau}$ and $\hat{\rho}_n$ is the shorthand notation for $\hat{\rho}(n\tau)$. The map $\mathcal{E}$ is a trace-preserving and completely positive quantum map. This kind of discrete quantum dynamics also occurs in so-called collision models [54], which in the short interaction time limit provide a dynamics that is equivalent to a Lindblad master equation.

The action of the map $\mathcal{E}$ is conveniently studied in terms of its right and left eigenmatrices, i.e., $\hat{R}_j$ and $\hat{L}_j$, and the corresponding eigenvalues λ_j [9]:

$$\hat{\rho}_n = \mathcal{E}^n\hat{\rho}_0 = \hat{\rho}_{ss} + \sum_{j\geqslant 1} \text{Tr}[\hat{L}_j\hat{\rho}_0]\hat{R}_j\lambda_j^n. \tag{3}$$

The eigenvalues satisfy $|\lambda_j| \leqslant 1$, and we arrange them in order of decreasing absolute value $|\lambda_0| \geqslant |\lambda_1| \geqslant |\lambda_2| \geqslant \ldots$. Those with unit absolute value correspond to nondecaying modes, while there is at least one stationary state that we denote as $\hat{\rho}_{ss} = \hat{R}_0/\text{Tr}[\hat{R}_0]$ with $\lambda_0 = 1$. It is also useful to define the frequencies and decay rates of the system as $\gamma_j\tau = -\ln[|\lambda_j|]$, $\nu_j\tau = \arg[\lambda_j]$, in analogy to the Liouvillian formalism [9,42]. Additionally, we will make use of spin coherent states, which provide the basis for a phase-space representation of the system state and operators. This
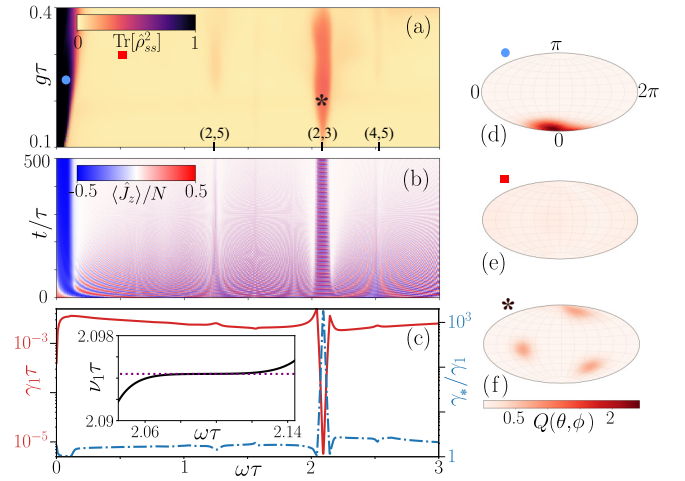

FIG. 2. Dynamical regimes and metastable resonances. (a) Purity of the stationary state as a function of g and ω. Three (p, q) resonances are marked. (b) Initial relaxation dynamics of the system magnetization with initial state $|J, J\rangle$, as a function of ω for $g\tau = 0.2$. (c) Red solid line: decay rate γ_1 of the leading excitation mode of the map $\mathcal{E}$ [see Eq. (2)] as a function of ω at $g\tau = 0.2$. Blue dashed-dotted line: ratio of the leading decay rate and the next (different) one, γ_* [for the $(p, q) = (2, 3)$ resonance this is $\gamma_* = \gamma_3$]. Inset: leading frequency, $\nu_1\tau$, of the metastable resonance. The dotted purple line corresponds to $\nu_1\tau = 2\pi/3$. (d)–(f) Aitoff projection of the Husimi Q function for $\hat{\rho}_{ss}$ and for the parameters indicated by the markers in (a): (d) $g\tau = 0.25$, $\omega\tau = 0.1$; (e) $g\tau = 0.3$, $\omega\tau = 0.5$; (f) $g\tau = 0.2$, $\omega\tau = 2\pi/3$. North to south pole: $\theta = \pi$ to $\theta = 0$. West to east: $\phi = 0$ to $\phi = 2\pi$. In all cases $N = 30$.

representation provides important insight on the different dynamical regimes of the model. For a spin J, coherent states are defined as $|\theta, \phi\rangle = \exp[i\theta(\hat{J}_x \sin\phi - \hat{J}_y \cos\phi)]|J, J\rangle$, where $\theta \in [0, \pi]$ and $\phi \in [0, 2\pi]$ define the polar and azimuthal angle, respectively [55]. Following [56], we will make use of the spin analogous of the Husimi Q function, defined for a spin operator $\hat{O}$ as $Q(\theta, \phi) = \mathcal{J}\langle\theta, \phi|\hat{O}|\theta, \phi\rangle$, where $\mathcal{J} = (2J + 1)/4\pi$ is a normalization constant.

III. RESULTS

A. Dynamical regimes and stationary purity

We find that for the study of the stationary state $\hat{\rho}_{ss}$ the purity is actually a good order parameter, noting that the magnetization, which appears to be the natural order parameter, is not sensitive to all dynamical regimes. The stationary purity is shown in Fig. 2(a) as a function of the Rabi frequency and interaction strength. For small $\omega\tau$, $\hat{\rho}_{ss}$ is almost pure, which follows from the interaction term dominating over the coherent driving, the former enforcing a stationary state close to $|J, -J\rangle$ [Fig. 2(d)]. In contrast, increasing $\omega\tau$ above a certain threshold makes the Rabi term dominate over the interaction one, changing qualitatively the stationary state. In this region, $\hat{\rho}_{ss}$ is a highly entropic mixed state, close to the infinite temperature state, and thus spreading out (quasi-)uniformly over the entire phase space [Fig. 2(e)]. For even larger $\omega\tau$, the interplay of coherent dynamics and periodic interruptions
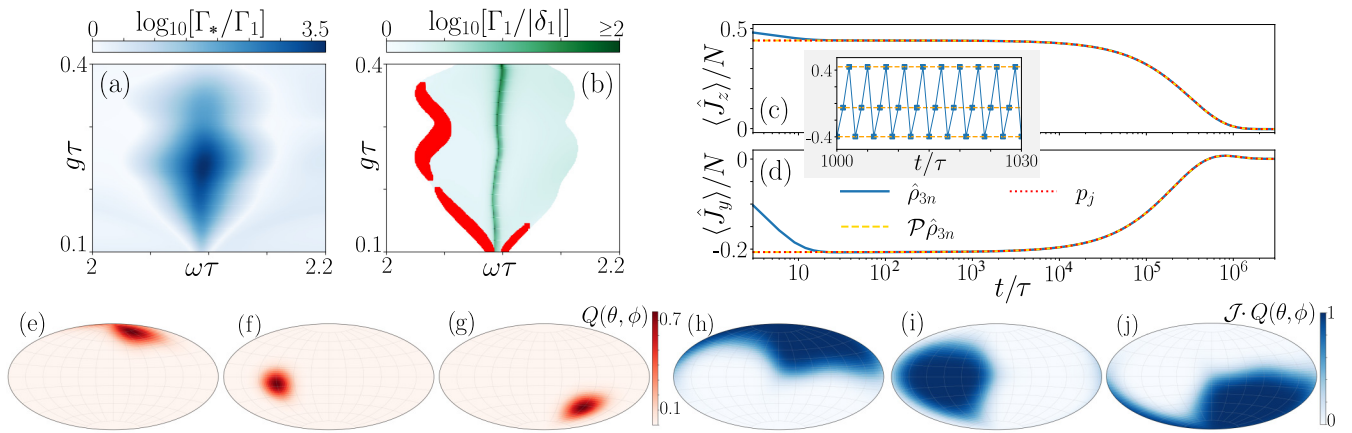
FIG. 3. Metastable dynamics. (a) Ratio of the leading decay rate, Γ_1, and the next (different) one, Γ_*, for the period-tripled stroboscopic map Λ. (b) Ratio of the leading decay rate and its corresponding detuning, δ_1, in the region in which the leading mode is complex. The regions in which $\Gamma_1/|\delta_1| < \sqrt{3}$ are colored in red. (c) and (d) Stroboscopic dynamics of the z and y components in the metastable regime considering the exact time evolution $\hat\rho_{3n}$ (blue solid line), the projection on the metastable manifold $\mathcal{P}\hat\rho_{3n}$ (yellow dashed line), and the classical stochastic model of Eq. (11) (red dotted line). Initial condition $|J, J\rangle$, $\omega\tau = 2\pi/3$, and $g\tau = 0.25$. Gray inset: the blue squares show the exact value of $\langle \hat{J}_z(n\tau)\rangle/N$, while the orange dashed lines show the values obtained from Eq. (10). Aitoff projection of the Husimi Q function for (e) $\hat\mu_1/3$; (f) $\hat\mu_2/3$; (g) $\hat\mu_3/3$; (h) $\hat{P}_1$; (i) $\hat{P}_2$; (j) $\hat{P}_3$. Parameters: $N = 30$, $\omega\tau = 2\pi/3$, $g\tau = 0.2$.

gives rise to yet another kind of dynamics: for $\omega\tau$ close to certain fractions of π, i.e., $p\pi/q$, purity islands emerge in which $\mathrm{Tr}[\hat\rho_{ss}^2] \sim 1/q$. In panel (a) these (p, q) resonances can be observed around $2\pi/5$, $2\pi/3$, and $4\pi/5$, the most prominent one being the one with $q = 3$. Near these metastable resonances the stationary state is a mixture of just q almost disjoint and highly pure states. This is to be contrasted with what happens generically outside these regions, where the system actually converges to an almost fully mixed (infinite temperature) stationary state. This suggests that in the metastable islands, due to a mechanism akin to ergodicity breaking, the system avoids heating up to infinite temperature. This is illustrated in Fig. 2(f) for $q = 3$ and in Appendix B for $q = 5$. In order to get an impression of the dynamics, we show in Fig. 2(b) the time evolution of the system spin magnetization $\langle \hat{J}_z \rangle$ for $g\tau = 0.2$. Here one finds that the purity islands labeled by (p, q) in panel (a) indeed correspond to metastable states, which display long-lived oscillations with a period that is approximately given by $T \approx q\tau$. This behavior is most evident around $(p, q) = (2, 3)$, although it can also be recognized near the other resonances [(2,5) and (4,5)]. In the following, we focus on the case $(p, q) = (2, 3)$, as the most prominent resonance in Fig. 2.

B. Metastable period-locking resonances

The observed long-lived oscillations can be characterized studying the leading eigenvalues of $\mathcal{E}$. In Fig. 2(c) we plot the leading decay rate of the system $\gamma_1\tau$ (red solid lines), observing that for the resonance around $\omega\tau = 2\pi/3$ this becomes several orders of magnitude smaller than anywhere else. At this resonance the eigenvalue λ_1 is complex and its corresponding frequency is plotted in the inset. This reveals a *frequency locking* to $\nu_1\tau \approx 2\pi/3$ across the entire $(2,3)$ resonance, a behavior that is reminiscent of the synchronization phenomenon of frequency entrainment. Here, the dominant frequency of a system also locks to a given

one in a whole dynamical regime, which has been observed both in classical [57] and quantum systems in [37,58,59]. In Fig. 2(c) we also plot the ratio of the dominant decay rate with the next (different) leading one (blue dotted line) [60]. This ratio increases by several orders of magnitude at the $(2,3)$ resonance, indicating the emergence of a huge separation of timescales: the long-time dynamics is thus dominated only by the two complex conjugated modes with frequency $|\nu_1|\tau \approx 2\pi/3$. This separation of timescales is characteristic of the emergence of metastability in open quantum systems [9]. Moreover, we find it to be present in the whole purity island, as shown in Fig. 3(a), giving rise to what we term as *metastable period-locking resonances*. Similar results can be found for resonances with higher q and different system sizes, in which more than two long-lived modes can be involved (see Appendix B).

This huge separation of timescales allows the metastable dynamics in the $(2,3)$ resonance to be approximated by [9]

$$\hat\rho_n \approx \hat\rho_{ss} + (c_1 \hat{R}_1 e^{i\nu_1 n\tau} + \mathrm{H.c.})e^{-\gamma_1 n\tau} = \mathcal{P}\hat\rho_n, \quad (4)$$

with $c_1 = \mathrm{Tr}[\hat{L}_1\hat\rho_0]$. The stationary state and these two longest-lived modes define the metastable manifold (MM), denoted by $\mathcal{P}\hat\rho_n$, to which the state of the system rapidly converges on a timescale given by γ_3^{-1}. Crucially, while $\gamma_1\tau \ll 1$, $\nu_1\tau$ is of order one. Therefore, in order to unveil the structure of the MM, it is more convenient to consider the *period-tripled stroboscopic map* $\Lambda = \mathcal{E}^3$, which displays the same eigenmatrices but with eigenvalues $\delta_j = 3\nu_j - 2\pi$ and $\Gamma_j = 3\gamma_j$. Thus, by switching to Λ, we have $\Gamma_1\tau \sim \delta_1\tau \ll 1$, as can be readily appreciated in Fig. 3(b). The metastable dynamics in this stroboscopic picture is exemplified in Figs. 3(c) and 3(d), in which its multistep character is evident: the system rapidly relaxes to the MM, in which the state appears to settle to $\hat\rho_{3n} \approx \mathcal{P}\hat\rho_0$ displaying a *metastable plateau* for intermediate times $\Gamma_3^{-1} \ll t \ll \Gamma_1^{-1}, |\delta_1^{-1}|$, until eventually reaching the true stationary state, described by Eq. (4).

C. Metastable symmetry broken states

The smallness of both Γ_1 and δ_1 shows that the metastable resonance manifests in the map Λ as a (quasi-)closure of the spectral gap, similarly to what is observed for finite sizes with the Liouvillian gap in DPTs [8,42]. As a consequence, the structure of the MM is analogous to that of the emerging stationary manifold for DPTs, analyzed in Ref. [42]. In fact, to a good approximation, the stationary state and the Hermitian partners of the leading eigenmodes [61] decompose in terms of the same three extremal metastable states (EMSs) [9], that allow us to write any state in the MM as a convex combination of them [see Eq. (8)]. These EMSs are denoted by $\hat{\mu}_{1,2,3}$ and given by

$$\hat{\rho}_{ss} \approx \frac{1}{3}(\hat{\mu}_1 + \hat{\mu}_2 + \hat{\mu}_3), \tag{5}$$

$$\hat{R}_A \approx \frac{c_A}{2}(2\hat{\mu}_1 - \hat{\mu}_2 - \hat{\mu}_3), \quad \hat{R}_B = c_B(\hat{\mu}_3 - \hat{\mu}_2). \tag{6}$$

Here $c_{A,B}$ are real constants corresponding to the sum of positive eigenvalues of $\hat{R}_{A,B}$, and in the whole metastable resonance their ratio is well approximated by $c_A/c_B \approx 2/\sqrt{3}$ (see Appendix A). In Figs. 3(e)–3(g) we show these EMSs, finding that they correspond to the different lobes making up the stationary state. The accuracy of these approximations is characterized in detail in Appendix A. Moreover, we observe the EMSs to be almost disjoint, as they are tightly focused in nonoverlapping phase-space regions. This can be better understood considering their left partners:

$$\hat{P}_1 = \frac{\mathbb{1}}{3} + c_A\hat{L}_A,$$

$$\hat{P}_2 = \frac{\mathbb{1}}{3} - \frac{c_A}{2}\hat{L}_A - c_B\hat{L}_B,$$

$$\hat{P}_3 = \frac{\mathbb{1}}{3} - \frac{c_A}{2}\hat{L}_A + c_B\hat{L}_B. \tag{7}$$

These Hermitian operators satisfy the following properties (see Appendix A): (i) $\hat{P}_1 + \hat{P}_2 + \hat{P}_3 = \mathbb{1}$; (ii) they are to a good approximation positive; and (iii) they satisfy to a good approximation $\text{Tr}[\hat{P}_j\hat{\mu}_k] = \delta_{jk}$. Accordingly, we can rewrite the projection of $\hat{\rho}_0$ in the MM as a probabilistic mixture of $\hat{\mu}_{1,2,3}$:

$$\mathcal{P}\hat{\rho}_0 \approx p_1^0\hat{\mu}_1 + p_2^0\hat{\mu}_2 + p_3^0\hat{\mu}_3, \tag{8}$$

with $p_j^0 = \text{Tr}[\hat{P}_j\hat{\rho}_0]$ which can be approximately regarded as classical probabilities. Inspecting the Husimi representation of $\hat{P}_j$, we find them to partition the phase space in three almost disjoint regions [Figs. 3(h)–3(j)]. These different regions correspond to the basin of attraction of each of the EMSs; any initial state contained in them will rapidly converge to the corresponding EMS and remain trapped in it for the long intermediate timescale.

The action of $\mathcal{E}$ on the EMSs unveils one of their most interesting features: they break (approximately) the discrete time-translation symmetry imposed by the periodic resetting of the central spin. Indeed, they are connected by $\mathcal{E}$ forming a period-tripled cyclic evolution:

$$\mathcal{E}\hat{\mu}_1 \approx \hat{\mu}_2, \quad \mathcal{E}\hat{\mu}_2 \approx \hat{\mu}_3, \quad \mathcal{E}\hat{\mu}_3 \approx \hat{\mu}_1. \tag{9}$$

These relations can be derived using Eqs. (5) and (6), and making the approximation $c_A/c_B \approx 2/\sqrt{3}$, $\Gamma_1 = \delta_1 \approx 0$ valid in the metastable resonance and for times $t \ll \Gamma_1^{-1} \sim |\delta_1|^{-1}$ (i.e., in the metastable plateau) (see Appendix A). Remarkably, the structure of Eq. (9) is analogous to that of conventional symmetry breaking DPTs [42] replacing the superoperator describing the symmetry, as, e.g., parity, by $\mathcal{E}$ [see Appendix B for an example with $(p, q) = (4, 5)$]. Finally, combining Eqs. (8) and (9), we see that in the metastable plateau the period-tripled dynamics is approximated by

$$\hat{\rho}_{3n+j} \approx p_1^0\hat{\mu}_{1+j} + p_2^0\hat{\mu}_{2+j} + p_3^0\hat{\mu}_{3+j}, \tag{10}$$

where $j = 0, 1, 2$ and the index of the metastable states follows periodic boundary conditions, i.e., $\hat{\mu}_4 = \hat{\mu}_1$. In the inset of Fig. 3(c) we consider the exact magnetization dynamics (blue squares) in the plateau and compare it with the three values predicted by this approximation (orange dashed lines), finding excellent agreement.

D. Effective nonequilibrium classical relaxation

The period-tripled oscillation eventually fades away due to the slow residual dynamics associated with the small but nonvanishing values of Γ_1 and δ_1. By rewriting Eq. (4) in terms of the EMSs, we find that this final relaxation (in the stroboscopic picture) follows a classical stochastic process, i.e., not only $\mathcal{P}\hat{\rho}_0$ can be written as a classical probabilistic mixture of the EMSs, but also $\mathcal{P}\hat{\rho}_{3n}$. Hence, we can promote Eq. (8) to $\mathcal{P}\hat{\rho}_{3n} \approx \sum_{j=1}^{3} p_j(n\tau)\hat{\mu}_j$, where the probabilities $p_j(t)$ obey (see Appendix A)

$$\frac{d}{dt}p_j = -\frac{2\Gamma_1}{3}p_j + \left(\frac{\Gamma_1}{3} - \frac{\delta_1}{\sqrt{3}}\right)p_{j+1} + \left(\frac{\Gamma_1}{3} + \frac{\delta_1}{\sqrt{3}}\right)p_{j-1}, \tag{11}$$

with initial condition p_j^0 and where the index j in (11) follows periodic boundary conditions. For the process (11) to be physical we need $\Gamma_1/|\delta_1| \geqslant \sqrt{3}$, which is satisfied in most of the metastable regime, except for the boundary regions indicated in red in Fig. 3(b). In Figs. 3(c) and 3(d) we exemplify these dynamics (red dotted lines), finding excellent agreement with the exact ones both in the plateau and in the final decay. An inspection of Eq. (11) reveals the stationary state to be $p_1 = p_2 = p_3 = 1/3$ as expected from Eq. (3). Interestingly, we find that stationary probability currents, given by $J_{j,j+1} = 2\delta_1/(3\sqrt{2})$ (see Appendix A), are generally present. This indicates the nonequilibrium nature of the final relaxation process of the metastable time-translation symmetry broken states, that contrasts with what was found for other quantum systems effectively governed in the long-time by infinite-temperature classical equilibrium process [9,34,37].

E. Dependence on the system size

We now analyze what happens to the metastable resonances when the size of the system is increased. As we shall see, these are also resonances in the system size, since their emergence strongly depends on the number of spins and their position in the phase diagram does not show a smooth behavior when this number is varied. This is illustrated in Fig. 4 in two different ways: first, by analyzing how the shape and the number of purity islands (associated with the metastable
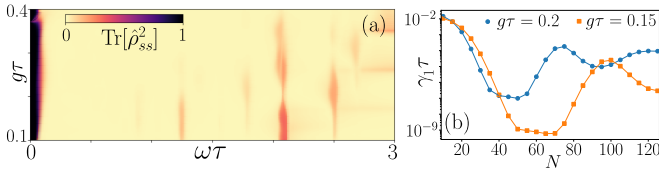
FIG. 4. Dependence on the system size. (a) Stationary purity $\text{Tr}[\hat{\rho}_{ss}^2]$ varying $g\tau$ and $\omega\tau$ for $N = 70$. (b) Decay rate of the dominant oscillatory mode in the (2,3) metastable resonance varying the system size and for $g\tau = 0.2$ (blue circles) or $g\tau = 0.15$ (orange squares) and $\omega\tau = 2\pi/3$.

resonances) change with system size, and then by studying the behavior of the lifetime of the dominant oscillatory mode when N is increased. In particular, in Fig. 4(a) we plot the same map as in Fig. 2(a) but considering a larger system size, i.e., $N = 70$. Comparing both figures, we observe that the number of islands as well as their shape change with N in a nontrivial way: for $N = 70$ we observe an increased number of purity islands, which, however, seem to shrink with increasing N (see Appendix C for other sizes). When considering the decay rate of the dominant oscillatory mode [Fig. 4(b)], i.e., that responsible for the main oscillations, we observe a nonmonotonic behavior with strong dependence on N. Such a nonmonotonic behavior is also observed for other metastable resonances with different p and q (see Appendix C). Thus, in contrast to dissipative phase transitions [42], there is no evidence for a closure of the spectral gap in the thermodynamic limit. The results of Fig. 4 rather suggest that these metastable resonances should be considered as many-body resonances, whose emergence necessitates a large enough system size, and which may move in the phase diagram or even disappear when increasing further the number of particles.

IV. CONCLUSION

We have reported on an intrinsically metastable counterpart of discrete time crystals, emerging in a dissipative spin model that may be regarded as the discrete-time generalization of the boundary time crystal of Ref. [18]. Similarly to prethermal [25–28] and metastable time crystals [29–33], these oscillations emerge in a prestationary regime, while their lifetime surpasses any intrinsic timescale of the model by orders of magnitude. Compared to other many-body ergodicity breaking dynamics, as due to dynamical symmetries [23] or quantum scars [62], the reported dynamics is largely independent on the initial conditions, as the EMSs act as effective attractors with a combined basin of attraction that spans all phase space. A further peculiarity is their nontrivial dependence on system size, as the largest lifetimes are attained for intermediate sizes resulting in a nonmonotonic behavior as the thermodynamic limit is approached. In fact, each of these resonances seem to display an optimal system size, as based on the smallness of dominant decay rate and on the extension of the purity island (see Figs. 4, 9, and 10), which suggests that they they do not develop into a standard nonequilibrium phase in the thermodynamic limit. Nevertheless, the fact that this spectral gap does not actually close does not preclude the emergence of a robust MM with a structure analogous to the

stationary one found in symmetry-breaking DPTs [42]. This points to a connection between time-translation symmetry breaking and other types of spontaneous symmetry breaking in driven-dissipative systems.

APPENDIX A: PERIOD-TRIPLED METASTABLE OSCILLATIONS

1. Long-time dynamics

We begin this section by writing down the long-time approximation for the dynamics in the period-tripled resonance:

$$\hat{\rho}_n \approx \hat{\rho}_{ss} + \text{Tr}[\hat{L}_1\hat{\rho}_0]\hat{R}_1 e^{i\nu_1 n\tau - \gamma_1 n\tau} + \text{H.c.} = \mathcal{P}\hat{\rho}_n. \quad (A1)$$

Notice that we stick to the following criteria for the definition of the eigenvalues and eigenmatrices: $\nu_1 > 0$ and $\text{Tr}[\hat{L}_1\hat{R}_1] = 1$. We want to rewrite Eq. (A1) in terms of the following Hermitian combinations of the long-lived eigenmodes:

$$\hat{R}_A = \frac{\hat{R}_1 + \hat{R}_1^\dagger}{2}, \quad \hat{R}_B = \frac{\hat{R}_1 - \hat{R}_1^\dagger}{2i},$$
$$\hat{L}_A = \hat{L}_1 + \hat{L}_1^\dagger, \quad \hat{L}_B = i(\hat{L}_1 - \hat{L}_1^\dagger), \quad (A2)$$

which satisfy $\text{Tr}[\hat{L}_j\hat{R}_k] = \delta_{jk}$ with $j, k = A, B$. We then obtain

$$\mathcal{P}\hat{\rho}_n = \hat{\rho}_{ss} + [A\cos(\nu_1 n\tau) + B\sin(\nu_1 n\tau)]\hat{R}_A e^{-\gamma_1 n\tau}$$
$$+ [B\cos(\nu_1 n\tau) - A\sin(\nu_1 n\tau)]\hat{R}_B e^{-\gamma_1 n\tau}, \quad (A3)$$

where $A = \text{Tr}[\hat{L}_A\hat{\rho}_0]$ and $B = \text{Tr}[\hat{L}_B\hat{\rho}_0]$. The advantage of $\hat{R}_{A,B}$ comes from the fact that they can be easily decomposed in terms of physical states as they are both Hermitian and traceless. Therefore, they are bound to satisfy

$$\hat{R}_A = \sum_{j=1}^{2J+1} a_j |A_j\rangle\langle A_j|, \quad \sum_{j=1}^{2J+1} a_j = 0,$$
$$\hat{R}_B = \sum_{j=1}^{2J+1} b_j |B_j\rangle\langle B_j|, \quad \sum_{j=1}^{2J+1} b_j = 0, \quad (A4)$$

where $2J + 1$ is the dimension of the Hilbert space in which the collective spin J resides. It is also useful to write the time evolution every three steps, i.e., in the stroboscopic period-tripled picture:

$$\mathcal{P}\hat{\rho}_{3n} = \hat{\rho}_{ss} + [A\cos(\delta_1 n\tau) + B\sin(\delta_1 n\tau)]\hat{R}_A e^{-\Gamma_1 n\tau}$$
$$+ [B\cos(\delta_1 n\tau) - A\sin(\delta_1 n\tau)]\hat{R}_B e^{-\Gamma_1 n\tau}, \quad (A5)$$

where $\delta_1 = 3\nu_1 - 2\pi$ and $\Gamma_1 = 3\gamma_1$.

2. Formal decomposition in stationary period-tripled lobes

In this section we will suppose that $\hat{R}_1$ and $\hat{R}_1^\dagger$ actually become eigenmodes with unit eigenvalue of the period-tripled map and explore the consequences of this. More precisely, we are assuming that $\Lambda \hat{R}_1 = \hat{R}_1$, $\Lambda \hat{R}_1^\dagger = \hat{R}_1^\dagger$ and thus $\Lambda \hat{R}_{A,B} = \hat{R}_{A,B}$ (recall $\Lambda = \mathcal{E}^3$). Then, $\hat{\rho}_{ss}$ and $\hat{R}_{A,B}$ all belong to the now *degenerate* stationary subspace of Λ. Notice that while $\hat{\rho}_{ss}$ and $\hat{R}_{A,B}$ need not be orthogonal, they are required to be linearly independent (in the vectorized representation). The other constraints to be satisfied are their unit or null trace, their Hermiticity, and the positivity of the stationary state. A possible way to satisfy these constraints is that they are all different linear combinations of a set of three stationary states. This crucial idea is one of the core results of Ref. [42]. Indeed, based on our numerical observations, we propose the following decomposition:

$$\hat{R}_A = \frac{c_A}{2}(2\hat{\mu}_1 - \hat{\mu}_2 - \hat{\mu}_3), \quad \hat{R}_B = c_B(\hat{\mu}_3 - \hat{\mu}_2),$$
$$\hat{\rho}_{ss} = \frac{1}{3}(\hat{\mu}_1 + \hat{\mu}_2 + \hat{\mu}_3), \tag{A6}$$

where $c_{A,B}$ are real constants. Hence, $\hat{\mu}_{1,2,3}$ are stationary states of Λ and linearly independent. This last property is better appreciated inverting (A6):

$$\hat{\mu}_1 = \hat{\rho}_{ss} + \frac{2\hat{R}_A}{3c_A},$$
$$\hat{\mu}_2 = \hat{\rho}_{ss} - \frac{\hat{R}_A}{3c_A} - \frac{\hat{R}_B}{2c_B},$$
$$\hat{\mu}_3 = \hat{\rho}_{ss} - \frac{\hat{R}_A}{3c_A} + \frac{\hat{R}_B}{2c_B}, \tag{A7}$$

which shows that they are an independent linear combination (nonzero determinant of the coefficients arranged in columns) of linearly independent vectors (the linear independence of $\hat{\rho}_{ss}$, $\hat{R}_A/c_A$, and $\hat{R}_B/c_B$ is guaranteed by the assumption that they are eigenmatrices of Λ). We can proceed in the same line for the left eigenmatrices, obtaining

$$\hat{P}_1 = \frac{\mathbb{1}}{3} + c_A \hat{L}_A, \quad \hat{P}_2 = \frac{\mathbb{1}}{3} - \frac{c_A \hat{L}_A}{2} - c_B \hat{L}_B,$$
$$\hat{P}_3 = \frac{\mathbb{1}}{3} - \frac{c_A \hat{L}_A}{2} + c_B \hat{L}_B, \tag{A8}$$

which satisfy

$$\hat{P}_1 + \hat{P}_2 + \hat{P}_3 = \mathbb{1}, \quad \text{Tr}[\hat{P}_j \hat{\mu}_k] = \delta_{jk} \quad \forall j,k, \tag{A9}$$

as follows by definition. Moreover, they must satisfy

$$\hat{P}_j \geqslant 0 \quad \forall j \tag{A10}$$

to guarantee that, whatever is the initial condition, $\mathcal{P}\hat{\rho}_0$ will be a positive semidefinite matrix. Indeed, from properties (A9) and (A10), it follows that

$$\mathcal{P}\hat{\rho}_0 = p_1^0 \hat{\mu}_1 + p_2^0 \hat{\mu}_2 + p_3^0 \hat{\mu}_3, \tag{A11}$$

with $p_j^0 = \text{Tr}[\hat{P}_j \hat{\rho}_0]$, and thus $p_j \geqslant 0$ and $p_1^0 + p_2^0 + p_3^0 = 1$. Therefore, $\mathcal{P}\hat{\rho}_0$ is a probability mixture of three stationary states, which motivates the term extreme metastable states (EMSs) [9]. We now address the question of whether $\hat{\mu}_{1,2,3}$

actually break the discrete time-translation symmetry of $\mathcal{E}$. Indeed, the result is that, if

$$r = \frac{c_A}{c_B} = \frac{2}{\sqrt{3}}, \tag{A12}$$

then

$$\mathcal{E}\hat{\mu}_1 = \hat{\mu}_2, \quad \mathcal{E}\hat{\mu}_2 = \hat{\mu}_3, \quad \mathcal{E}\hat{\mu}_3 = \hat{\mu}_1. \tag{A13}$$

Notice that our initial assumption that $\Lambda \hat{R}_1 = \hat{R}_1$ implies that $\nu_1 = 2\pi/3$. Then $\mathcal{E}R_1 = (-1/2 + i\sqrt{3}/2)\hat{R}_1$, and together with (A12) we obtain

$$\mathcal{E}\left[\frac{\hat{R}_A}{c_A}\right] = -\frac{\hat{R}_A}{2c_A} - \frac{3\hat{R}_B}{4c_B},$$
$$\mathcal{E}\left[\frac{\hat{R}_B}{c_B}\right] = \frac{\hat{R}_A}{c_A} - \frac{\hat{R}_B}{2c_B}, \tag{A14}$$

which can be used to obtain the cyclic relation (A13).

3. Approximate decomposition in metastable period-tripled lobes

In our system $\delta_1 \tau \ll 1$, $\Gamma_1 \tau \ll 1$, although they are nonzero. This means that the results of the previous section do not apply exactly but only in an approximate way. The most straightforward way to obtain an approximation for $\hat{\mu}_{1,2,3}$ is to use the spectral decomposition of $\hat{R}_{A,B}$. Indeed, we can choose

$$\hat{\mu}_2 = \frac{1}{c_B} \sum_{b_j < 0} b_j |B_j\rangle\langle B_j|, \quad c_B = \sum_{b_j > 0} b_j,$$
$$\hat{\mu}_3 = \frac{1}{c_B} \sum_{b_j > 0} b_j |B_j\rangle\langle B_j|, \tag{A15}$$
$$\hat{\mu}_1 = \frac{1}{c_A} \sum_{a_j > 0} a_j |A_j\rangle\langle A_j|, \quad c_A = \sum_{a_j > 0} a_j, \tag{A16}$$

which ensures that $\hat{\mu}_{1,2,3}$ are bona fide density matrices. However, then we have that some of the following relations hold under the approximation sign:

$$\hat{R}_A \approx \frac{c_A}{2}(2\hat{\mu}_1 - \hat{\mu}_2 - \hat{\mu}_3), \quad \hat{R}_B = c_B(\hat{\mu}_3 - \hat{\mu}_2),$$
$$\hat{\rho}_{ss} \approx \frac{1}{3}(\hat{\mu}_1 + \hat{\mu}_2 + \hat{\mu}_3) = \xi, \tag{A17}$$

and their accuracy needs to be checked. Moreover, we will also find that Eqs. (A11) and (A12) also apply only approximately, while $\text{Tr}[\hat{P}_j \hat{\mu}_k] \approx \delta_{jk}$ and they are only approximately positive. Therefore, the accuracy of such approximations needs to be characterized for the metastable region. This is done in Fig. 5, in which we characterize the main approximations: (a) the trace distance between the actual stationary state and its approximation; (b) the trace distance between $\mathcal{E}\hat{\mu}_1$ and $\hat{\mu}_2$; (c) the largest negative eigenvalue of $\hat{P}_1$ denoted by λ_N; and (d) the deviation of r from $2/\sqrt{3}$, denoted by Δr. Comparing these results with those of Fig. 3(a) of the main text, we observe that the larger is Γ_*/Γ_1, the better are these approximations. We conclude that these approximate results
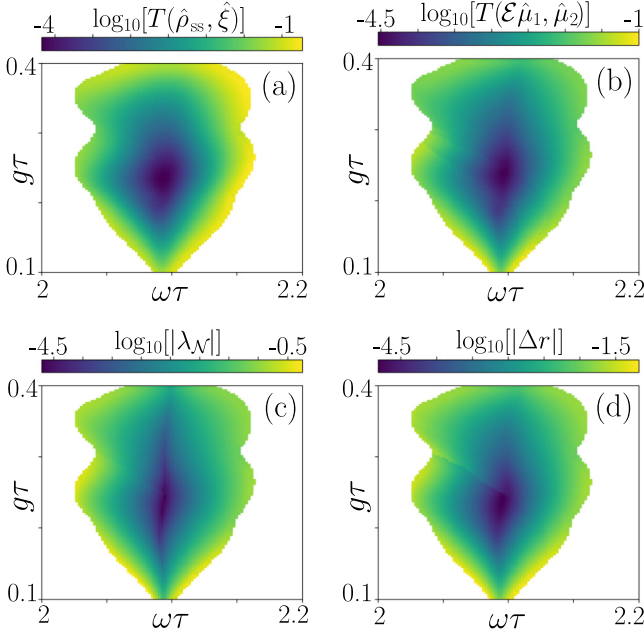
FIG. 5. Characterization of the main approximations in the metastable period-tripled regime for $N = 30$. The plots are restricted to the region in which the dominant eigenmodes are the complex conjugate ones leading to period tripling. All plots are in logarithmic scale. (a) Trace distance between the actual stationary state and its approximation given by Eq. (A17). (b) Trace distance between $\mathcal{E}\hat{\mu}_1$ and $\hat{\mu}_2$. (c) Absolute value of the largest negative eigenvalue of $\hat{P}_1$, denoted by $\lambda_{\mathcal{N}}$. (d) Absolute value of the difference between the actual value of r and the theoretical one, i.e., $2/\sqrt{3}$. Here $\Delta r = r - 2/\sqrt{3}$.

are in good agreement with the exact ones for the relevant metastable region.

4. Classical relaxation dynamics

A remarkable result is that not only $\mathcal{P}\hat{\rho}_0$ can be approximated as a probabilistic mixture of three metastable states, but the entire relaxation dynamics of $\mathcal{P}\hat{\rho}_{3n}$ can be described by a classical three-state stochastic process. In order to show this, we will make use of the rescaled Hermitian modes and their left partners which we define as

$$\hat{R}'_{A,B} = \frac{\hat{R}_{A,B}}{c_{A,B}}, \quad \hat{L}'_{A,B} = c_{A,B}\hat{L}_{A,B}. \quad \text{(A18)}$$

Rewriting the stroboscopic dynamics given by Eq. (A5) in terms of the rescaled Hermitian modes we obtain

$$\mathcal{P}\hat{\rho}_{3n} = \hat{\rho}_{ss} + [A'\cos(\delta_1 n\tau) + rB'\sin(\delta_1 n\tau)]\hat{R}'_A e^{-\Gamma_1 n\tau}$$
$$+ [B'\cos(\delta_1 n\tau) - \frac{A'}{r}\sin(\delta_1 n\tau)]\hat{R}'_B e^{-\Gamma_1 n\tau}, \quad \text{(A19)}$$

where $A' = \text{Tr}[\hat{L}'_A\hat{\rho}_0]$ and $B' = \text{Tr}[\hat{L}'_B\hat{\rho}_0]$. Then, we make use of the expression of the eigenmodes in terms of the EMSs given in Eq. (A17) to obtain

$$\mathcal{P}\hat{\rho}(3n\tau) \approx p_1(n\tau)\hat{\mu}_1 + p_2(n\tau)\hat{\mu}_2 + p_3(n\tau)\hat{\mu}_3, \quad \text{(A20)}$$

where the $p_j(n\tau)$ are given in terms of only the initial conditions p_j^0 and the rates Γ_1 and δ_1:

$$p_1(n\tau) = \frac{p_1^0}{3}[1 + 2\cos(\delta_1 n\tau)e^{-\Gamma_1 n\tau}]$$
$$+ \frac{p_3^0}{3}(1 - [\cos(\delta_1 n\tau) - \sqrt{3}\sin(\delta_1 n\tau)]e^{-\Gamma_1 n\tau})$$
$$+ \frac{p_2^0}{3}(1 - [\cos(\delta_1 n\tau) + \sqrt{3}\sin(\delta_1 n\tau)]e^{-\Gamma_1 n\tau}), \quad \text{(A21)}$$

$$p_2(n\tau) = \frac{p_2^0}{3}[1 + 2\cos(\delta_1 n\tau)e^{-\Gamma_1 n\tau}]$$
$$+ \frac{p_1^0}{3}(1 - [\cos(\delta_1 n\tau) - \sqrt{3}\sin(\delta_1 n\tau)]e^{-\Gamma_1 n\tau})$$
$$+ \frac{p_3^0}{3}(1 - [\cos(\delta_1 n\tau) + \sqrt{3}\sin(\delta_1 n\tau)]e^{-\Gamma_1 n\tau}), \quad \text{(A22)}$$

$$p_3(n\tau) = \frac{p_3^0}{3}[1 + 2\cos(\delta_1 n\tau)e^{-\Gamma_1 n\tau}]$$
$$+ \frac{p_2^0}{3}(1 - [\cos(\delta_1 n\tau) - \sqrt{3}\sin(\delta_1 n\tau)]e^{-\Gamma_1 n\tau})$$
$$+ \frac{p_1^0}{3}(1 - [\cos(\delta_1 n\tau) + \sqrt{3}\sin(\delta_1 n\tau)]e^{-\Gamma_1 n\tau}). \quad \text{(A23)}$$

Notice that here we have used the approximations $c_A/c_B \approx 2/\sqrt{3}$, Eq. (A17), and the expression of p_j^0 in terms of A' and B', which can be obtained from their definition $p_j^0 = \text{Tr}[\hat{P}_j\hat{\rho}_0]$ and read

$$p_1^0 = \frac{1}{3} + A', \quad p_2^0 = \frac{1}{3} - \frac{A'}{2} - B', \quad p_3^0 = \frac{1}{3} - \frac{A'}{2} + B'. \quad \text{(A24)}$$

The use of these approximations is the reason why we write Eq. (A20) under the approximate sign. Finally, we recognize (i.e., we can check) that Eqs. (A21)–(A23) are indeed the solution at discrete time steps $t = n\tau$ of the classical stochastic process given by

$$\frac{d}{dt}p_1 = -\frac{2\Gamma_1}{3}p_1 + \left(\frac{\Gamma_1}{3} - \frac{\delta_1}{\sqrt{3}}\right)p_2 + \left(\frac{\Gamma_1}{3} + \frac{\delta_1}{\sqrt{3}}\right)p_3, \quad \text{(A25)}$$

$$\frac{d}{dt}p_2 = -\frac{2\Gamma_1}{3}p_2 + \left(\frac{\Gamma_1}{3} - \frac{\delta_1}{\sqrt{3}}\right)p_3 + \left(\frac{\Gamma_1}{3} + \frac{\delta_1}{\sqrt{3}}\right)p_1, \quad \text{(A26)}$$

$$\frac{d}{dt}p_3 = -\frac{2\Gamma_1}{3}p_3 + \left(\frac{\Gamma_1}{3} - \frac{\delta_1}{\sqrt{3}}\right)p_1 + \left(\frac{\Gamma_1}{3} + \frac{\delta_1}{\sqrt{3}}\right)p_2, \quad \text{(A27)}$$

with initial conditions p_j^0. Notice that the condition for these equations to represent a classical stochastic process is that

$$\frac{\Gamma_1}{|\delta_1|} \geqslant \sqrt{3}, \quad \text{(A28)}$$

since the off-diagonal rates need to be positive. From Fig. 3(b) of the main text, we see that this condition is widely satisfied. Then, Eqs. (A25)–(A27) guarantee that $p_j(t)$ can be regarded as probabilities at all times. This process generalizes to three states the effective classical dynamics disclosed in Refs. [9,34]. We observe that when considering three states, there is the possibility to have a very slow oscillation in the long-time relaxation as described by the terms proportional to δ_1.

5. Stationary current

The classical stochastic process given by Eqs. (A25)–(A27) can be written in matrix form:

$$\frac{d}{dt}\vec{p} = W\vec{p}, \tag{A29}$$

where $\vec{p} = (p_1, p_2, p_3)^T$ and

$$W = \begin{pmatrix} -\frac{2\Gamma_1}{3} & \frac{\Gamma_1}{3} - \frac{\delta_1}{\sqrt{3}} & \frac{\Gamma_1}{3} + \frac{\delta_1}{\sqrt{3}} \\ \frac{\Gamma_1}{3} + \frac{\delta_1}{\sqrt{3}} & -\frac{2\Gamma_1}{3} & \frac{\Gamma_1}{3} - \frac{\delta_1}{\sqrt{3}} \\ \frac{\Gamma_1}{3} - \frac{\delta_1}{\sqrt{3}} & \frac{\Gamma_1}{3} + \frac{\delta_1}{\sqrt{3}} & -\frac{2\Gamma_1}{3} \end{pmatrix}. \tag{A30}$$

The matrix W satisfies the following properties that guarantee it to be a classical stochastic process: (i) the sum of each of the columns is zero, i.e., $\sum_{i=1}^{3} W_{ij} = 0 \ \forall j$, which guarantees conservation of probability; (ii) the off-diagonal elements are positive semidefinite (if $\Gamma_1 \geqslant \sqrt{3}|\delta_1|$), i.e., $W_{ij} \geqslant 0$ if $i \neq j$, which guarantees the p_j's to remain positive. Moreover, a third property (iii) is that the sum of the elements of the same row is zero, i.e., $\sum_{j=1}^{3} W_{ij} = 0 \ \forall i$, which indicates that the stationary state is uniform, i.e., $p_1^\infty = p_2^\infty = p_3^\infty = 1/3$. Despite the stationary state is uniform, it displays nonzero currents and thus it is a *nonequilibrium* stationary state. The stationary current from state i to state j is given by

$$J_{ij} = p_i^\infty W_{ji} - p_j^\infty W_{ij}, \tag{A31}$$

from which we find that

$$J = J_{12} = J_{23} = J_{31} = \frac{2\delta_1}{3\sqrt{3}}. \tag{A32}$$

Thus if $\delta_1 > 0$, there is a stationary clockwise probability current, while if $\delta_1 < 0$ there is a stationary anticlockwise probability current.

APPENDIX B: PERIOD-5 METASTABLE OSCILLATIONS

1. Long-time dynamics

Besides the prominent $p = 2$, $q = 3$ region in which we have focused, we can also find other types of metastable resonances. In particular, a second important one is that occurring for $p = 4$ and $q = 5$. While signatures of this resonance in the stationary state are already evident for $N = 30$, i.e., $\text{Tr}[\hat{\rho}_{ss}^2] \sim 1/5$ and $\hat{\rho}_{ss}$ made of five disjoint lobes, this becomes more important in systems with larger sizes. For instance, in Fig. 6(a), we exemplify the dynamics for $N = 70$ varying $\omega\tau$ and for a cut at $g\tau = 0.18$, similarly to what we have done in the main text. We can appreciate both the transition from overdamped to underdamped dynamics as well as the presence of metastable resonances for several combinations of (p, q),
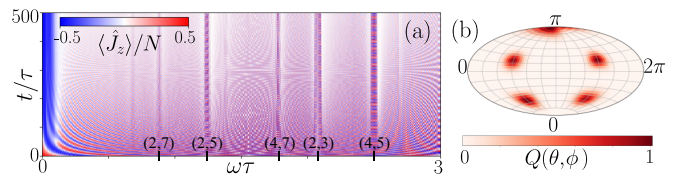

FIG. 6. (a) Magnetization dynamics varying the Rabi frequency and for an exemplary cut at $g\tau = 0.18$, with the initial condition $|J, J\rangle$ and system size $N = 70$. In the horizontal axis we have marked the most prominent metastable resonances, where the notation (p, q) resonance stands for a resonance around the frequency $\omega = p\pi/q$. (b) Aitoff projection of the Husimi Q function for the stationary state in the (4,5) resonance. The parameters are $\omega\tau = 4\pi/5$, $g\tau = 0.18$, and $N = 70$.

the (4,5) resonance being particularly clear. In panel (b) we plot the stationary state for a point inside the (4,5) resonance, finding that it displays five almost disjoint lobes, as anticipated in the main text.

In the (4,5) resonance we find the long-time dynamics to be accurately described by

$$\hat{\rho}_n \approx \hat{\rho}_{ss} + \text{Tr}[\hat{L}_1\hat{\rho}_0]\hat{R}_1 e^{i\nu_1 n\tau - \gamma_1 n\tau}$$
$$+ \text{Tr}[\hat{L}_2\hat{\rho}_0]\hat{R}_2 e^{i\nu_2 n\tau - \gamma_2 n\tau} + \text{H.c.} = \mathcal{P}_5\hat{\rho}_n. \tag{B1}$$

Notice that we stick to the following criteria for the definition of the eigenvalues and eigenmatrices: $\nu_1 > 0$, $\nu_2 > 0$, $\text{Tr}[\hat{L}_1\hat{R}_1] = 1$, and $\text{Tr}[\hat{L}_2\hat{R}_2] = 1$. Moreover, in this resonance, we typically find that $\gamma_1 \sim \gamma_2$, while $\nu_1\tau \sim 4\pi/5$ and $\nu_2\tau \sim 2\pi/5$. As in the period-tripled case, we will work with the Hermitian counterparts of the long-lived eigenmodes:

$$\hat{R}_A = \frac{\hat{R}_1 + \hat{R}_1^\dagger}{2}, \quad \hat{R}_B = \frac{\hat{R}_1 - \hat{R}_1^\dagger}{2i},$$
$$\hat{R}_C = \frac{\hat{R}_2 + \hat{R}_2^\dagger}{2}, \quad \hat{R}_D = \frac{\hat{R}_2 - \hat{R}_2^\dagger}{2i}, \tag{B2}$$
$$\hat{L}_A = \hat{L}_1 + \hat{L}_1^\dagger, \quad \hat{L}_B = i(\hat{L}_1 - \hat{L}_1^\dagger),$$
$$\hat{L}_C = \hat{L}_2 + \hat{L}_2^\dagger, \quad \hat{L}_D = i(\hat{L}_2 - \hat{L}_2^\dagger), \tag{B3}$$

which satisfy $\text{Tr}[\hat{L}_j\hat{R}_k] = \delta_{jk}$ with $j, k \in \{A, B, C, D\}$. Since they are Hermitian and traceless, we can decompose them as the subtraction of two physical states:

$$\hat{R}_X = \sum_{j=1}^{2J+1} x_j |X_j\rangle\langle X_j|, \quad \sum_{j=1}^{2J+1} x_j = 0, \quad \text{with } x = a, b, c, d. \tag{B4}$$

Importantly, this decomposition allows us to define the following constants:

$$c_X = \sum_{x_j > 0} x_j, \quad \text{with } x = a, b, c, d. \tag{B5}$$

2. Formal decomposition in period-5 lobes

We consider now the period-5 map $\Lambda_5 = \mathcal{E}^5$, which displays the same eigenmatrices but whose eigenvalues are a factor 5 those of $\mathcal{E}$. We suppose that this map displays a gap closure in the region $p = 4$, $q = 5$, in which $\Gamma_{1,2} = 0$ and $\delta_{1,2} = 0$, and we propose a decomposition of the involved
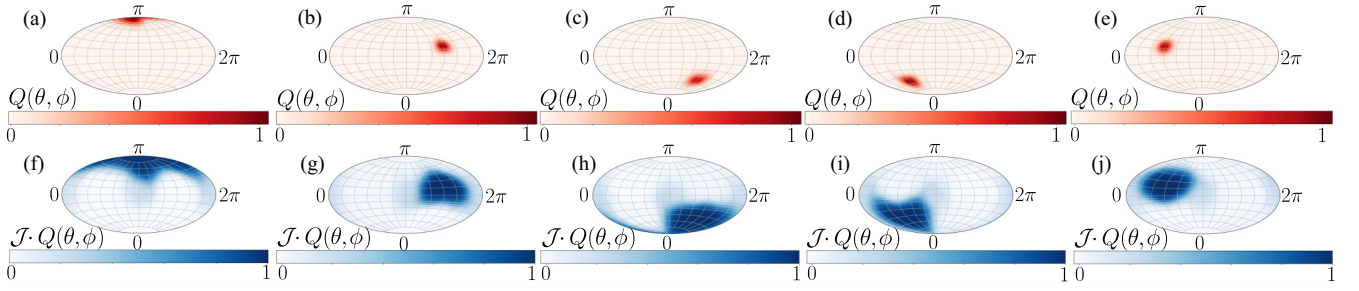
FIG. 7. Aitoff projection of the Husimi Q function of the period-5 lobes and their left partners for $N = 70$, $g\tau = 0.18$, and $\omega\tau = 4\pi/5$. (a)–(e) Metastable lobes: $\hat{\mu}_1/5$ to $\hat{\mu}_5/5$, respectively. (f)–(j) Left projectors: $\hat{P}_1$ to $\hat{P}_5$, respectively. For these parameters the leading decay rates and frequencies are given by $\gamma_1\tau = 1.3 \times 10^{-5}$, $\nu_1\tau = 2.5133$; $\gamma_2\tau = 3.2 \times 10^{-5}$, $\nu_2\tau = 1.2566$; while the next mode has $\gamma_*\tau = 3.9 \times 10^{-4}$, $\nu_*\tau = 0$, with $* = 5$ as there are two pairs of long-lived metastable modes. In this case we have a ratio of $\gamma_*/\gamma_2 = 12.2$ between the largest rate of the metastable manifold and the next one. Moreover, we obtain the following values for the figures of merit: $T(\mathcal{E}\hat{\mu}_j, \hat{\mu}_{j+2}) \approx 0.033$, while the smallest eigenvalue of $\hat{P}_j$ takes values around $\lambda_\mathcal{N} \approx -0.02$. Finally, due to the way in which we have defined the metastable lobes and projectors, we have that the definitions in Eqs. (B6)–(B10) and $\mathrm{Tr}[\hat{P}_j\hat{\mu}_k] = \delta_{jk}$ are satisfied exactly (and thus the corresponding trace distances are zero).

modes in terms of a set of period-5 states. Numerical observation leads us to propose the following decomposition:

$$\hat{\rho}_{ss} = \frac{1}{5}(\hat{\mu}_1 + \hat{\mu}_2 + \hat{\mu}_3 + \hat{\mu}_4 + \hat{\mu}_5), \qquad (B6)$$

$$\hat{R}_A = \frac{c_A}{5}(3\hat{\mu}_1 + \hat{\mu}_2 + \hat{\mu}_5) - \frac{c_A}{2}(\hat{\mu}_3 + \hat{\mu}_4), \qquad (B7)$$

$$\hat{R}_B = \frac{c_B}{5}(3\hat{\mu}_5 + 2\hat{\mu}_4 - 3\hat{\mu}_2 - 2\hat{\mu}_3), \qquad (B8)$$

$$\hat{R}_C = \frac{c_C}{5}(3\hat{\mu}_1 + \hat{\mu}_3 + \hat{\mu}_4) - \frac{c_C}{2}(\hat{\mu}_2 + \hat{\mu}_5), \qquad (B9)$$

$$\hat{R}_D = \frac{c_D}{5}(2\hat{\mu}_2 + 3\hat{\mu}_4 - 3\hat{\mu}_3 - 2\hat{\mu}_5). \qquad (B10)$$

We then obtain the following expressions for the different lobes:

$$\hat{\mu}_1 = \hat{\rho}_{ss} + \frac{2}{3}(\hat{R}'_A + \hat{R}'_C), \qquad (B11)$$

$$\hat{\mu}_2 = \hat{\rho}_{ss} + \frac{1}{546}(104\hat{R}'_A - 315\hat{R}'_B - 286\hat{R}'_C + 210\hat{R}'_D), \qquad (B12)$$

$$\hat{\mu}_3 = \hat{\rho}_{ss} + \frac{1}{546}(-286\hat{R}'_A - 210\hat{R}'_B + 104\hat{R}'_C - 315\hat{R}'_D), \qquad (B13)$$

$$\hat{\mu}_4 = \hat{\rho}_{ss} + \frac{1}{546}(-286\hat{R}'_A + 210\hat{R}'_B + 104\hat{R}'_C + 315\hat{R}'_D), \qquad (B14)$$

$$\hat{\mu}_5 = \hat{\rho}_{ss} + \frac{1}{546}(104\hat{R}'_A + 315\hat{R}'_B - 286\hat{R}'_C - 210\hat{R}'_D), \qquad (B15)$$

where we have defined $\hat{R}'_X = \hat{R}_X/c_X$, with X = A, B, C, D. Similarly as in the period-tripled case, we also define their left partners as

$$\hat{P}_1 = \frac{1}{5}(\mathbb{1} + 3\hat{L}'_A + 3\hat{L}'_C), \qquad (B16)$$

$$\hat{P}_2 = \frac{1}{5}(\mathbb{1} + \hat{L}'_A - 3\hat{L}'_B + 2\hat{L}'_D) - \frac{\hat{L}'_C}{2}, \qquad (B17)$$

$$\hat{P}_3 = \frac{1}{5}(\mathbb{1} - 2\hat{L}'_B + \hat{L}'_C - 3\hat{L}'_D) - \frac{\hat{L}'_A}{2}, \qquad (B18)$$

$$\hat{P}_4 = \frac{1}{5}(\mathbb{1} + 2\hat{L}'_B + \hat{L}'_C + 3\hat{L}'_D) - \frac{\hat{L}'_A}{2}, \qquad (B19)$$

$$\hat{P}_5 = \frac{1}{5}(\mathbb{1} + \hat{L}'_A + 3\hat{L}'_B - 2\hat{L}'_D) - \frac{\hat{L}'_C}{2}, \qquad (B20)$$

where we have defined $\hat{L}'_X = c_X\hat{L}_X$, with X = A, B, C, D. These operators satisfy

$$\sum_{j=1}^{5} \hat{P}_j = \mathbb{1}, \qquad \mathrm{Tr}[\hat{P}_i\hat{\mu}_j] = \delta_{ij}. \qquad (B21)$$

Here we notice that the positivity of $\hat{P}_i$ and $\hat{\mu}_i$ is interrelated. If there was an actual gap closure and thus $\hat{\mu}_i$ were true stationary states we would necessarily have $\hat{P}_i \geqslant 0$.

3. Approximate decomposition in period-5 lobes

For the period-5 case we follow a slightly different strategy to define the approximate EMSs than in the period-tripled case. Instead of defining them from the spectral decomposition of the Hermitian partners of the eigenmodes, we define them through the relations given in Eqs. (B6)–(B10). In principle, if there was an actual gap closure both ways would provide equivalent results. However, in practice this means that instead of $\hat{\mu}_j$ being bona fide states and Eqs. (A17) holding approximately, we now have it the other way around: Eqs. (B6)–(B10) hold exactly; however, $\hat{\mu}_j$ and their left partners display small corrections to positivity. The reason why here we proceed in this different way is that, due to the increased complexity of the MM, this is the most straightforward manner of isolating the metastable lobes. Nevertheless, we recall that if the approximation is good, such differences remain small. As we will show now, these metastable approximations also work well for the period-5 case.

In Fig. 7 we exemplify this lobe decomposition, from which we can appreciate that the EMSs correspond to the lobes making up the stationary state shown in Fig. 6(b). Here, we also check for the period-5 cyclic relation connecting the

EMSs, which we numerically find to be

$$\mathcal{E}\hat{\mu}_1 \approx \hat{\mu}_3, \quad \mathcal{E}\hat{\mu}_2 \approx \hat{\mu}_4, \quad \mathcal{E}\hat{\mu}_3 \approx \hat{\mu}_5,$$
$$\mathcal{E}\hat{\mu}_4 \approx \hat{\mu}_1, \quad \mathcal{E}\hat{\mu}_5 \approx \hat{\mu}_2. \quad \text{(B22)}$$

Regarding the corrections to these approximations, we find the smallest eigenvalue of the $\hat{P}_j$ to take values around $\lambda_{\mathcal{N}} \approx -0.02$, while trace distances for the cyclic relation take values around $T(\mathcal{E}\hat{\mu}_j, \hat{\mu}_{j+2}) \approx 0.033$. Comparing this with the results for the period-tripled case shown in Fig. 5, we see that the corrections in the period-5 case are generally larger. This is in agreement with the fact that the spectral gap between the eigenvalues of the MM and the smallest ones outside it is smaller compared to the period-tripled case, taking the value $\gamma_*/\gamma_2 = 12.2$ for the chosen parameters. As we shall see, although the corrections for these approximations are larger, we still find good agreement when looking at the dynamics (see next section). This good agreement can be in part attributed to the immediate leading eigenmodes outside the MM not playing an important role for the z and y components of the magnetization dynamics.

4. Approximate metastable dynamics

In this section we want to compare the exact dynamics with the approximate ones for the (4,5) resonance. In particular, a first level of approximation is given by Eq. (B1), in which we have neglected the contributions of modes outside the MM for long times. In Figs. 8(a)–8(d) we compare this approximation (in gold dashed lines and triangles) with the exact dynamics (blue solid lines and circles), finding that after a short initial transient both display excellent agreement. A further level of approximation consists in approximating the state of the system in the metastable plateau by the initial probabilistic mixture of EMSs:

$$\mathcal{P}_5\hat{\rho}_0 \approx p_1^0\hat{\mu}_1 + p_2^0\hat{\mu}_2 + p_3^0\hat{\mu}_3 + p_4^0\hat{\mu}_4 + p_5^0\hat{\mu}_5, \quad \text{(B23)}$$

where $p_j^0 = \text{Tr}[\hat{P}_j\hat{\rho}_0]$. Indeed, the z and y components of the magnetization according to Eq. (B23) are shown in Figs. 8(a) and 8(b) in red dotted lines, finding excellent agreement within the metastable plateau; that is, after an initial short transient and before the final decay takes place. Moreover, making use of Eq. (B22) we can approximate the period-5 dynamics inside the plateau as

$$\hat{\rho}_{5n+j} \approx p_1^0\hat{\mu}_{1+2j} + p_2^0\hat{\mu}_{2+2j} + p_3^0\hat{\mu}_{3+2j}$$
$$+ p_4^0\hat{\mu}_{4+2j} + p_5^0\hat{\mu}_{5+2j}, \quad \text{(B24)}$$

where $j = 0, 1, 2, 3, 4$ and the index of the metastable states follows periodic boundary conditions, i.e., $\hat{\mu}_{5+k} = \hat{\mu}_{\text{mod}(5+k,5)}$ with $k \geqslant 1$. In Figs. 8(e) and 8(f) we compare the exact oscillatory dynamics (blue circles) with the approximation given in Eq. (B24) (red triangles). We notice that the agreement is not so good as for the same approximation done in the period-tripled case (main text), although differences between exact dynamics and this approximation are still reasonably small. The fact that this kind of approximation does not work so well as in the period-tripled case can be traced back to Eq. (B22) also not working so well (see also caption of Fig. 7),
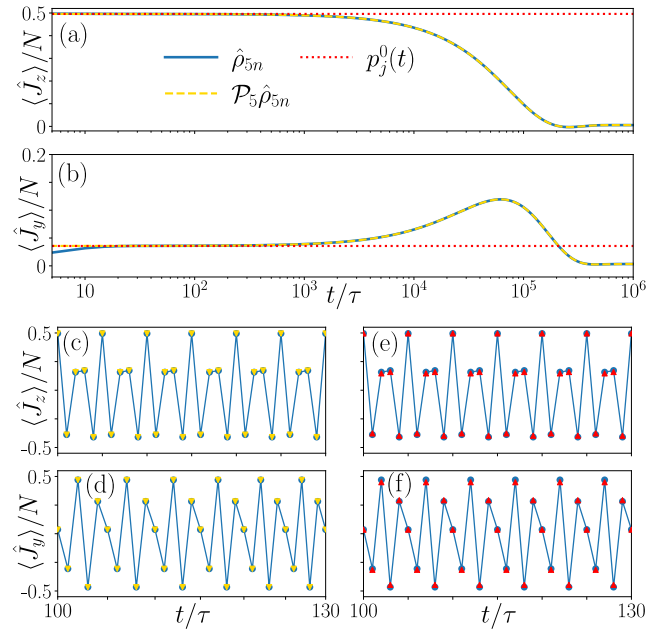

FIG. 8. (a), (b) Stroboscopic period-5 dynamics for the magnetization in the z and y directions. Exact results in blue solid lines. In gold dashed lines, results according to the projection onto the MM as given by Eq. (B1). In red dotted lines, initial incoherent mixture as given by Eq. (B23). Initial condition $|J, J\rangle$. Parameters: $N = 70$, $g\tau = 0.18$, and $\omega\tau = 4\pi/5$. (c)–(f) Zoom in of the oscillatory dynamics for an interval of time in the metastable plateau. (c), (d) Comparison of the approximation given by Eq. (B1) (gold down triangles) with the exact results (blue circles). (e), (f) Comparison of the approximation given by Eq. (B24) (red up triangles) with the exact results (blue circles). Same parameters and initial condition as in (a) and (b).

which as we have already commented it can in turn be traced back to the spectral gap between the MM and the rest of the eigenmodes being not so accentuated as in the (2,3) resonance studied in the main text.

In conclusion, besides quantitative differences in the level of precision of these approximations, we find our main results to apply also for this case. The only result that we have not generalized to this higher-order resonance is a (possible) classical stochastic process describing the final relaxation in a stroboscopic picture.
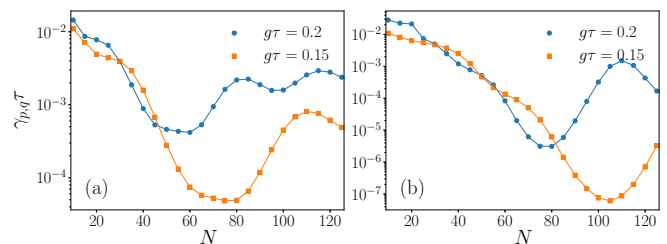

FIG. 9. Decay rate of the dominant oscillatory mode in the (p, q) metastable resonance, $\gamma_{p,q}$, varying the system size and for $g\tau = 0.2$ (blue circles) or $g\tau = 0.15$ (orange squares). (a) $\omega\tau = 2\pi/5$. (b) $\omega\tau = 4\pi/5$.
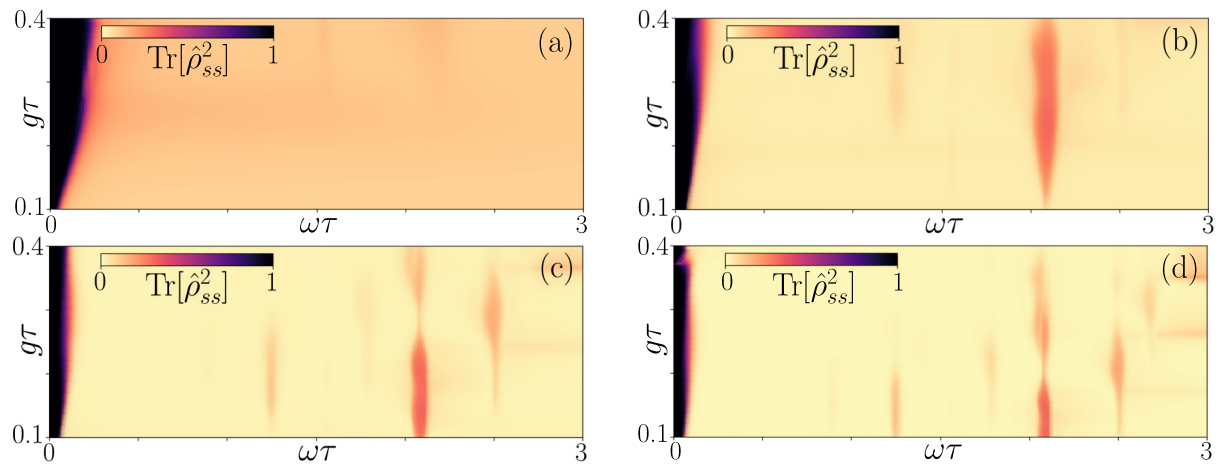
FIG. 10. Comparison of the stationary purity $\text{Tr}[\hat{\rho}_{ss}^2]$ varying $g\tau$ and $\omega\tau$ for different system sizes: (a) $N = 10$, (b) $N = 30$, (c) $N = 50$, and (d) $N = 70$.

APPENDIX C: ADDITIONAL RESULTS FOR DIFFERENT SYSTEM SIZES

In this Appendix we present additional results complementing those of the main text regarding the effect of increasing the system size. In particular, in Fig. 9 we consider two values of $g\tau$ and we plot $\gamma_{p,q}$ for a Rabi frequency ω in (a) the (2,5) resonance and (b) the (4,5) resonance. In both the cases the results are qualitatively the same as those displayed in the main text: the decay rate of the dominant oscillatory mode displays a nonmonotonic behavior and oscillations with system size. As a second complementary result, in Fig. 10 we reproduce in the same plot the purity maps for (a) $N = 10$, (b)

$N = 30$, (c) $N = 50$, and (d) $N = 70$, in order to ease the visualization of how the purity islands change with system size. Notice how the background color becomes clearer progressively, as the minimum attainable purity is $1/N$. For $N = 10$, we can observe that the region for larger Rabi frequencies is almost uniform, not displaying purity islands. In the rest of the cases, purity islands are clearly visible. As commented in the main text, the number of islands increases with system size while at the same time they change position and seem to shrink or span smaller regions of parameter space. These results further illustrate how the metastable resonances do not smoothly approach a thermodynamic limit, but that they rather are also resonances in system size.

[1] S. Diehl, A. Micheli, A. Kantian, B. Kraus, H. P. Büchler, and P. Zoller, Quantum states and phases in driven open quantum systems with cold atoms, Nat. Phys. **4**, 878 (2008).

[2] S. Diehl, A. Tomadin, A. Micheli, R. Fazio, and P. Zoller, Dynamical Phase Transitions and Instabilities in Open Atomic Many-Body Systems, Phys. Rev. Lett. **105**, 015702 (2010).

[3] T. E. Lee, S. Gopalakrishnan, and M. D. Lukin, Unconventional Magnetism via Optical Pumping of Interacting Spin Systems, Phys. Rev. Lett. **110**, 257204 (2013).

[4] J. Jin, D. Rossini, R. Fazio, M. Leib, and M. J. Hartmann, Photon Solid Phases in Driven Arrays of Nonlinearly Coupled Cavities, Phys. Rev. Lett. **110**, 163605 (2013).

[5] M. Marcuzzi, E. Levi, S. Diehl, J. P. Garrahan, and I. Lesanovsky, Universal Nonequilibrium Properties of Dissipative Rydberg Gases, Phys. Rev. Lett. **113**, 210401 (2014).

[6] M. Marcuzzi, M. Buchhold, S. Diehl, and I. Lesanovsky, Absorbing State Phase Transition with Competing Quantum and Classical Fluctuations, Phys. Rev. Lett. **116**, 245701 (2016).

[7] G. Buonaiuto, F. Carollo, B. Olmos, and I. Lesanovsky, Dynamical Phases and Quantum Correlations in an Emitter-Waveguide System with Feedback, Phys. Rev. Lett. **127**, 133601 (2021).

[8] E. M. Kessler, G. Giedke, A. Imamoglu, S. F. Yelin, M. D. Lukin, and J. I. Cirac, Dissipative phase transition in a central spin system, Phys. Rev. A **86**, 012116 (2012).

[9] K. Macieszczak, M. Guta, I. Lesanovsky, and J. P. Garrahan, Towards a Theory of Metastability in Open Quantum Dynamics, Phys. Rev. Lett. **116**, 240404 (2016).

[10] W. Casteels, R. Fazio, and C. Ciuti, Critical dynamical properties of a first-order dissipative phase transition, Phys. Rev. A **95**, 012128 (2017).

[11] W. Casteels, F. Storme, A. Le Boité, and C. Ciuti, Power laws in the dynamic hysteresis of quantum nonlinear photonic resonators, Phys. Rev. A **93**, 033824 (2016).

[12] F. Wilczek, Quantum Time Crystals, Phys. Rev. Lett. **109**, 160401 (2012).

[13] P. Bruno, Comment on "Quantum Time Crystals", Phys. Rev. Lett. **110**, 118901 (2013).

[14] H. Watanabe and M. Oshikawa, Absence of Quantum Time Crystals, Phys. Rev. Lett. **114**, 251603 (2015).

[15] D. V. Else, B. Bauer, and C. Nayak, Floquet Time Crystals, Phys. Rev. Lett. **117**, 090402 (2016).

[16] V. Khemani, A. Lazarides, R. Moessner, and S. L. Sondhi, Phase Structure of Driven Quantum Systems, Phys. Rev. Lett. **116**, 250401 (2016).

[17] N. Y. Yao, A. C. Potter, I.-D. Potirniche, and A. Vishwanath, Discrete Time Crystals: Rigidity, Criticality, and Realizations, Phys. Rev. Lett. **118**, 030401 (2017).

[18] F. Iemini, A. Russomanno, J. Keeling, M. Schirò, M. Dalmonte, and R. Fazio, Boundary Time Crystals, Phys. Rev. Lett. **121**, 035301 (2018).

[19] Z. Gong, R. Hamazaki, and M. Ueda, Discrete Time-Crystalline Order in Cavity and Circuit QED Systems, Phys. Rev. Lett. **120**, 040404 (2018).

[20] K. Tucker, B. Zhu, R. J. Lewis-Swan, J. Marino, F. Jimenez, J. G. Restrepo, and A. M. Rey, Shattered time: can a dissipative time crystal survive many-body correlations? New J. Phys. **20**, 123003 (2018).

[21] R. R. W. Wang, B. Xing, G. G. Carlo, and D. Poletti, Period doubling in period-one steady states, Phys. Rev. E **97**, 020202(R) (2018).

[22] F. M. Gambetta, F. Carollo, M. Marcuzzi, J. P. Garrahan, and I. Lesanovsky, Discrete Time Crystals in the Absence of Manifest Symmetries or Disorder in Open Quantum Systems, Phys. Rev. Lett. **122**, 015701 (2019).

[23] B. Buča, J. Tindall, and D. Jaksch, Non-stationary coherent quantum many-body dynamics through dissipation, Nat. Commun. **10**, 1730 (2019).

[24] K. Chinzei and T. N. Ikeda, Time Crystals Protected by Floquet Dynamical Symmetry in Hubbard Models, Phys. Rev. Lett. **125**, 060601 (2020).

[25] D. V. Else, B. Bauer, and C. Nayak, Prethermal Phases of Matter Protected by Time-Translation Symmetry, Phys. Rev. X **7**, 011026 (2017).

[26] F. Machado, D. V. Else, G. D. Kahanamoku-Meyer, C. Nayak, and N. Y. Yao, Long-Range Prethermal Phases of Nonequilibrium Matter, Phys. Rev. X **10**, 011043 (2020).

[27] D. V. Else, C. Monroe, C. Nayak, and N. Y. Yao, Discrete time crystals Annu. Rev. Condens. Matter Phys. **11**, 467 (2020).

[28] A. Kyprianidis, F. Machado, W. Morong, P. Becker, K. S. Collins, D. V. Else, L. Feng, P. W. Hess, C. Nayak, G. Pagano, N. Y. Yao, and C. Monroe, Observation of a prethermal discrete time crystal, Science **372**, 1192 (2021).

[29] B. Zhu, J. Marino, N. Y. Yao, M. D. Lukin, and E. A. Demler, Dicke time crystals in driven-dissipative quantum many-body systems, New J. Phys. **21**, 073028 (2019).

[30] H. Keßler, P. Kongkhambut, C. Georges, L. Mathey, J. G. Cosme, and A. Hemmerich, Observation of a Dissipative Time Crystal, Phys. Rev. Lett. **127**, 043602 (2021).

[31] R. J. L. Tuquero, J. Skulte, L. Mathey, and J. G. Cosme, Dissipative time crystal in an atom-cavity system: Influence of trap and competing interactions, Phys. Rev. A **105**, 043311 (2022).

[32] S. Sarkar and Y. Dubi, Emergence and dynamical stability of a charge time-crystal in a current-carrying quantum dot simulator, Nano Lett. **22**, 4445 (2022).

[33] S. Sarkar and Y. Dubi, Signatures of discrete time-crystallinity in transport through an open Fermionic chain, Commun. Phys. **5**, 155 (2022).

[34] D. C. Rose, K. Macieszczak, I. Lesanovsky, and J. P. Garrahan, Metastability in an open quantum Ising model, Phys. Rev. E **94**, 052132 (2016).

[35] A. Le Boité, M.-J. Hwang, and M. B. Plenio, Metastability in the driven-dissipative Rabi model, Phys. Rev. A **95**, 023829 (2017).

[36] S. Wolff, A. Sheikhan, S. Diehl, and C. Kollath, Nonequilibrium metastable state in a chain of interacting spinless fermions with localized loss, Phys. Rev. B **101**, 075139 (2020).

[37] A. Cabot, G. L. Giorgi, and R. Zambrini, Metastable quantum entrainment, New J. Phys. **23**, 103017 (2021).

[38] K. Macieszczak, D. C. Rose, I. Lesanovsky, and J. P. Garrahan, Theory of classical metastability in open quantum systems, Phys. Rev. Res. **3**, 033047 (2021).

[39] A. Labay-Mora, R. Zambrini, and G. L. Giorgi, Quantum associative memory with a single driven-dissipative non-linear oscillator, arXiv:2205.09491.

[40] M. Fitzpatrick, N. M. Sundaresan, A. C. Y. Li, J. Koch, and A. A. Houck, Observation of a Dissipative Phase Transition in a One-Dimensional Circuit QED Lattice, Phys. Rev. X **7**, 011016 (2017).

[41] T. Fink, A. Schade, S. Höfling, C. Schneider, and A. Imamoglu, Signatures of a dissipative phase transition in photon correlation measurements, Nat. Phys. **14**, 365 (2018).

[42] F. Minganti, A. Biella, N. Bartolo, and C. Ciuti, Spectral theory of Liouvillians for dissipative phase transitions, Phys. Rev. A **98**, 042118 (2018).

[43] I. Lesanovsky and J. P. Garrahan, Kinetic Constraints, Hierarchical Relaxation, and Onset of Glassiness in Strongly Interacting and Dissipative Rydberg Gases, Phys. Rev. Lett. **111**, 215305 (2013).

[44] D. C. Rose, K. Macieszczak, I. Lesanovsky, and J. P. Garrahan, Hierarchical classical metastability in an open quantum East model, Phys. Rev. E **105**, 044121 (2022).

[45] A. Cabot, G. L. Giorgi, F. Galve, and R. Zambrini, Quantum Synchronization in Dimer Atomic Lattices, Phys. Rev. Lett. **123**, 023604 (2019).

[46] G. L. Giorgi, A. Cabot, and R. Zambrini, Transient synchronization in open quantum systems, in *Advances in Open Systems and Fundamental Tests of Quantum Mechanics*, edited by B. Vacchini, H.-P. Breuer, and A. Bassi (Springer, Cham), pp. 73–89.

[47] J. Tindall, C. Sánchez Muñoz, B. Buča, and D. Jaksch, Quantum synchronisation enabled by dynamical symmetries and dissipation, New J. Phys. **22**, 013026 (2020).

[48] B. Urbaszek, X. Marie, T. Amand, O. Krebs, P. Voisin, P. Maletinsky, A. Högele, and A. Imamoglu, Nuclear spin physics in quantum dots: An optical investigation, Rev. Mod. Phys. **85**, 79 (2013).

[49] I. Schwartz, J. Scheuer, B. Tratzmiller, S. Müller, Q. Chen, I. Dhand, Z.-Y. Wang, C. Müller, B. Naydenov, F. Jelezko, and M.-B. Plenio, Robust optical polarization of nuclear spin baths using Hamiltonian engineering of nitrogen-vacancy center quantum dynamics, Sci. Adv. **4**, eaat8978 (2018).

[50] M. Bortz and J. Stolze, Exact dynamics in the inhomogeneous central-spin model, Phys. Rev. B **76**, 014304 (2007).

[51] T. Villazon, A. Chandran, and P. W. Claeys, Integrability and dark states in an anisotropic central spin model, Phys. Rev. Res. **2**, 032052(R) (2020).

[52] T. Villazon, P. W. Claeys, M. Pandey, A. Polkovnikov, and A. Chandran, Persistent dark states in anisotropic central spin models, Sci. Rep. **10**, 16080 (2020).

[53] E. M. Kessler, S. Yelin, M. D. Lukin, J. I. Cirac, and G. Giedke, Optical Superradiance from Nuclear Spin Environment of Single-Photon Emitters, Phys. Rev. Lett. **104**, 143601 (2010).

[54] F. Ciccarello, S. Lorenzo, V. Giovannetti, and G. Massimo Palma, Quantum collision models: Open system dynamics from repeated interactions, Phys. Rep. **954**, 1 (2022).

[55] J. Ma, X. Wanga, C. P. Suna, and F. Nori, Quantum spin squeezing, Phys. Rep. **509**, 89 (2011).

[56] A. Roulet and C. Bruder, Synchronizing the Smallest Possible System, Phys. Rev. Lett. **121**, 053601 (2018).

[57] A. S. Pikovsky, M. Rosenblum, and J. Kurths, *Synchronization: A Universal Concept in Nonlinear Science* (Cambridge University Press, New York, 2001).

[58] S. Walter, A. Nunnenkamp, and C. Bruder, Quantum Synchronization of a Driven Self-Sustained Oscillator, Phys. Rev. Lett. **112**, 094102 (2014).

[59] S. Sonar, M. Hajdušek, M. Mukherjee, R. Fazio, V. Vedral, and S. Vinjanampathy, Squeezing Enhances Quantum Synchronization, Phys. Rev. Lett. **120**, 163601 (2018).

[60] We denote the next (different) leading rate as γ_*. In the $(2, 3)$ resonance $\gamma_* = \gamma_3$ as $\lambda_2 = \lambda_1^*$.

[61] We define $\hat{R}_A = (\hat{R}_1 + \hat{R}_1^\dagger)/2$, $\hat{R}_B = (\hat{R}_1 - \hat{R}_1^\dagger)/(2i)$, $\hat{L}_A = \hat{L}_1 + \hat{L}_1^\dagger$, and $\hat{L}_B = i(\hat{L}_1 - \hat{L}_1^\dagger)$.

[62] M. Serbyn, D. A. Abanin, and Z. Papić, Quantum many-body scars and weak breaking of ergodicity, Nat. Phys. **17**, 675 (2021).